Lift of a bio-inspired flapping wing with a dynamic trailing-edge flap in forward flight ⊘

Chen Yixin (陈一鑫) ⓘ ; Wang Chunyu (王春雨) ⓘ ; Zhao Jingshan (赵景山) ✉ ⓘ ;
Wang Shizhao (王士召) ✉ ⓘ

Check for updates

View Online

Export Citation

Lift of a bio-inspired flapping wing with a dynamic trailing-edge flap in forward flight

Yixin Chen (陈一鑫),[1,2] [iD] Chunyu Wang (王春雨),[1,2] [iD] Jingshan Zhao (赵景山),[3,a] [iD] and Shizhao Wang (王士召)[1,2,a] [iD]

AFFILIATIONS

[1]The State Key Laboratory of Nonlinear Mechanics, Institute of Mechanics, Chinese Academy of Sciences, Beijing 100190, China
[2]School of Engineering Sciences, University of Chinese Academy of Sciences, Beijing 101408, China
[3]The State Key Laboratory of Tribology, Department of Mechanical Engineering, Tsinghua University, Beijing 100084, China

[a]Authors to whom correspondence should be addressed: jingshanzhao@mail.tsinghua.edu.cn and wangsz@lnm.imech.ac.cn

ABSTRACT

Unlike the tail of a bird, regarded as a separately controlled aerodynamic surface, the membrane tail of a bat is operated as a dynamic trailing-edge flap. We investigate the effects of a dynamic trailing-edge flap on unsteady lift by numerically solving the Navier–Stokes equations around a bio-inspired flapping wing. The peak of the lift coefficient in the downstroke is considerably affected by the phase difference between the dynamic trailing-edge flap and the elevation. A quasi-steady formula is proposed to model the effects of phase difference on lift. The model is consistent with numerical results and experimental observations.

Published under an exclusive license by AIP Publishing. https://doi.org/10.1063/5.0146636

The brown long-eared bat (*Plecotus auritus*) and the Noack's roundleaf bat (*Hipposideros ruber*) have a distinct uropatagium (tail membrane) that connects to the legs and forms an extension to the plagiopatagium (the membrane connecting the arms, digits, and legs),[1,2] as shown in Fig. 1(a). The motion of the legs causes active deformation of both the uropatagium and the plagiopatagium. It has been hypothesized that the aerodynamic performance of the bat uropatagium is similar to that of a bird tail,[3–8] but recent experimental results have shown that the uropatagium might have additional aerodynamic functions.[9,10] Adams *et al.* note that the uropatagium provides additional thrust during takeoffs and slow flight.[11] Gardiner *et al.*[10] and Ramezani *et al.*[12] report that the uropatagium of bats plays a beneficial role in increasing lift, as well as reducing drag and controlling pitching moment.

Through biologists' recordings of the uropatagium in bat flight, the camber of the uropatagium is found to be affected actively by leg motion in the dorsoventral direction.[1,13] The legs move ventrally during the downstroke and move dorsally during the upstroke.[14] The phase difference between the uropatagium motion and the plagiopatagium motion leads to a periodical change in the camber of the membrane. The uropatagium can be modeled as a dynamic trailing-edge flap connected to the main wing. The effects of the uropatagium on the aerodynamic forces can be accomplished by introducing a dynamic trailing-edge flap to a flapping-wing model.

In this Letter, we use a bio-inspired flapping-wing model to investigate the role of the uropatagium motion in forward flight. The bio-inspired flapping-wing model is adapted from models used in previous literature,[15–18] which accounts for the dynamic trailing-edge flap associated with the motion of the uropatagium, as well as the elevating and sweep morphing of the plagiopatagium, as shown in Fig. 1(a). The schematic of the bio-inspired flapping-wing model is shown in Fig. 1(b). The modeled wing is divided into an inner wing *ABCD* and an outer wing *CDE*. The spanwise lengths of the inner and outer wings are b_1 and b_2, respectively. The sweep angles of the inner and outer wings are Λ_1 and Λ_2, respectively. The wing rotates around the root, as shown in Fig. 1(c). The elevating angles of the inner and outer wings are Ψ_1 and Ψ_2, respectively. The chordwise length at the wing root is *c*. The dynamic trailing-edge flap associated with the uropatagium is modeled by the motion of the triangle *ABC*. The triangle *ABC* rotates around the line *AC* during flapping. Figure 1(d) shows the spanwise profile of the inner wing to illustrate how the morphing uropatagium is achieved. In the spanwise profile *LIT*, all points on *IT* rotate around the point *I*. The angle between the lines *IT* and *IL* is the pitching angle of the dynamic trailing-edge flap α. The deformed spanwise profile *LIT* is measured by an effective angle α_{eff}, which is defined by the angle between the line *LT* and the line *LI*, as shown in Fig. 1(d).

Point *A* of the bio-inspired flapping-wing model was fixed in a uniform upstream flow. The kinematics of the flapping flight is described in a fixed coordinate system of *o–xyz*, where the *o–x* axis is
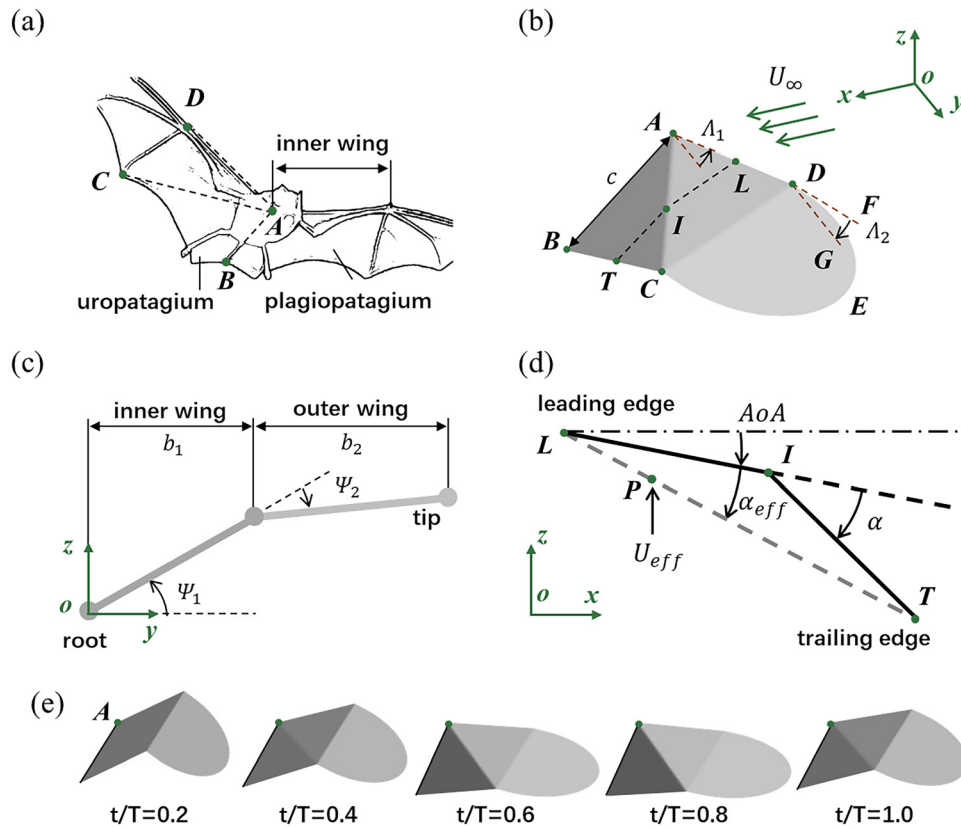
FIG. 1. (a) Schematic diagram of bat membrane (perspective view from the ventral), adapted from the work of Hendenström and Johansson.[2] (b) Schematic diagram of flapping wing with elevating and pitching (perspective view from the dorsal), where U_∞ denotes uniform upstream velocity. (c) Sketch of the elevating kinematics. (d) Profile of the inner wing. P is the quarter-chord point of the effective airfoil LT. The effective velocity U_{eff} is the z-direction velocity of the global coordinate relative to point P. (e) Snapshots of the half wing at different time (perspective view from the dorsal).

parallel to the uniform upstream flow, the o–y axis goes along the wingspan, and o–z axis is parallel to the vertical direction, as shown in Figs. 1(b) and 1(c). According to the work of Wang $et\ al.,$[15] we take $b_1 = b_2 = c$, and $\Lambda_1 = 0.35$ rad. For the inner and outer wing flapping, the specific settings of the elevating angle in Fig. 1(c) are given as follows:

$$\Psi_1(t) = 0.20 + 0.40 \sin(2\pi ft), \tag{1}$$

$$\Psi_2(t) = 0.35 + 0.30 \sin(2\pi ft), \tag{2}$$

where $f = 0.24$ is the dimensionless frequency. All the variables in this Letter are dimensionless, and are normalized by the reference length c, uniform upstream velocity U_∞, and the fluid density ρ. The sweep morphing of the outer wing is set as

$$\Lambda_2 = 0.30 \sin(2\pi ft). \tag{3}$$

For the motion of the uropatagium, the dynamic trailing-edge flap is specified as

$$\alpha(t) = \alpha_0 + \alpha_m \sin(2\pi ft + \pi - \varphi), \tag{4}$$

where α_0 is the mean angle of the dynamic trailing-edge flap, α_m is the amplitude of the dynamic trailing-edge flap, and φ is the phase difference between the dynamic trailing-edge flap and the rotation around

the root; φ controls the time difference between the dynamic trailing-edge flap and the elevating motion into the downstroke. For example, when $\varphi = 0°$, the uropatagium and the inner wing start the downstroke and upstroke at the same time; when $\varphi = 180°$, the inner wing starts the downstroke and the uropatagium starts the upstroke.

The unsteady flows and aerodynamic forces of the flapping-wing model are obtained by numerically solving the Navier–Stokes equation for incompressible flow by using an in-house code. We set the Reynolds number at $Re = U_\infty c/\nu = 300$, where ν is the fluid kinematic viscosity, with the assumption that separation at the sharp leading-edge is not sensitive to the Reynolds number, in accordance with previous work.[15,19–21] Details of the numerical method and validations can be found in our previous paper.[21–23] Limited by the length of this Letter, this work focuses on the unsteady lift influenced by the dynamic trailing-edge flap associated with the uropatagium morphing.

We take the phase differences in Eq. (4) as $-45°$, $0°$, $45°$, $90°$, $135°$, and $180°$. At the same time, we take the mean angle of attack (AoA) at $25°$ and $\alpha_0 = \alpha_m = 10°$ for the movement of the dynamic trailing-edge flap. To investigate the effects of the dynamic trailing-edge flap, we also simulated a baseline case without uropatagium morphing, where $\alpha_0 = \alpha_m = 0°$. The lift coefficient of the model is defined as
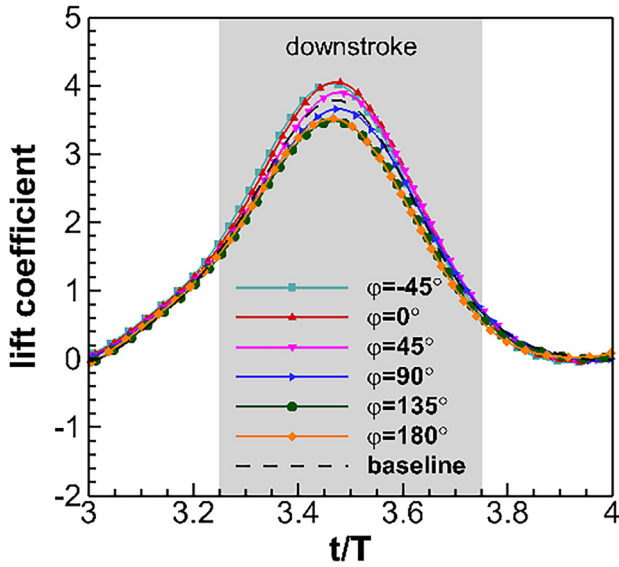
FIG. 2. Lift coefficients at different phase differences. The gray and white blocks denote the downstroke and upstroke, respectively.

$$C_L = \frac{L}{\frac{1}{2}\rho U_\infty^2 S^*}, \qquad (5)$$

where S^* is the area of the entire wing, and L is the lift. Figure 2 shows the lift coefficient at different phase differences of the dynamic trailing-edge flap compared to that of the baseline case. The lift coefficients for the two cases with $\varphi = 0°$ and $-45°$ are close to each other and higher than those of the other cases. The lift coefficients for the two cases with $\varphi = 180°$ and $135°$ are close to each other and lower than those of the other cases. The result shows that it is beneficial to increase lift when the start time of the downstroke of the dynamic trailing-edge flap and the elevating motion is close.

The results in Fig. 2 indicate that the dynamic trailing-edge flap with appropriate phase difference can increase the peak lift coefficient on the downstroke. We also investigate the effects of the dynamic trailing-edge flap at different α_0, α_m, and AoA to confirm that the relationship between φ and C_L still holds for different parameters. Figure 3 shows the lift coefficients corresponding to the phase difference ($\varphi = 0°$ and $\varphi = 180°$), while setting different AoA or amplitudes of dynamic trailing-edge flap α_m. In Fig. 3(a), α_m changes, and all the cases are fixed at $AoA = 10°$. When $\alpha_0 = \alpha_m = 20°$, the lift coefficient of the case with $\varphi = 0°$ is greatly improved during the downstroke compared with the case with $\alpha_0 = \alpha_m = 10°$, but the lift coefficient of the case with $\varphi = 180°$ does not vary noticeably on the downstroke with the change of amplitude. The lift peak of the case with $\varphi = 180°$ is very close to the baseline at the same AoA, and its lift coefficient is only slightly improved during the upstroke owing to the greater amplitude. From Fig. 3(b), it can be noted that the lift coefficient corresponding to the case with $\varphi = 0°$ is higher than those corresponding to the case with $\varphi = 180°$ for both angles of attack in Fig. 3(b), whether $AoA = 25°$ or $AoA = 10°$. Thus, the relationship between φ and C_L cannot be affected by amplitude, the mean angle of the dynamic trailing-edge flap, or AoA.

To quantify the amount of chordwise deformation in a similar manner to that evaluated by Li et al.[24] and Dai et al.,[25] an effective airfoil and effective pitching angle are introduced, as illustrated in Fig. 1(d). The quarter-chord point P is approximated here as the aerodynamic center of the effective airfoil LT. To account for the effect of the dynamic trailing-edge flap on the motion of the inner wing (more details of the considerations can be found in the supplementary material), we define the z-direction velocity of the global coordinate relative to point P at the spanwise position $y = 0.25$ as the effective velocity U_{eff}. The effective velocity can be expressed as

$$U_{eff}(t/T, \varphi) = -\frac{d\Psi_1}{dt} y \cos \Psi_1$$
$$+ \frac{d[\alpha_{eff}(t/T, \varphi)]}{dt} \frac{l}{4} \cos[\alpha_{eff}(t/T, \varphi) + AoA], \quad (6)$$
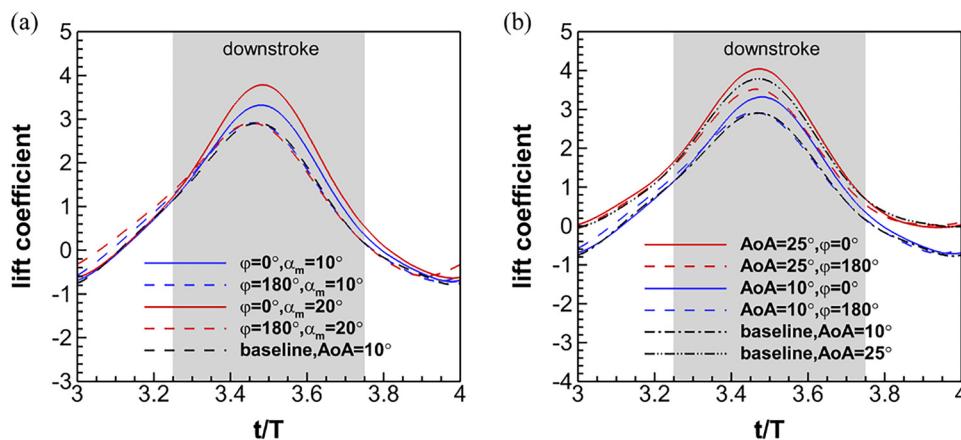

FIG. 3. Lift coefficient curves with two types of phase difference $\varphi = 0°$ and $\varphi = 180°$ after changing the amplitude of the dynamic trailing-edge flap α_m or AoA, where the baseline denotes no dynamic trailing-edge flap, with changes in AoA only. The gray and white blocks denote the downstroke and upstroke, respectively. (a) Changing the amplitude α_m for two types of phase difference. (b) Changing AoA for two types of phase difference.

where AoA is the angle of attack, which is a constant for the wing model used in this work. l is the chord length of the effective airfoil LT. Equation (6) shows that U_{eff} consists of the flapping of the inner wing and the pitching of the effective airfoil, respectively. The detail of the derivation of Eq. (6) can be found in the supplementary material.

It can be seen from Fig. 4 that the z-direction relative velocity of point P at the spanwise position $y = 0.25$ shows a similar trend in magnitude for the phase difference cases of the lift curves. It can be seen that the U_{eff} curve for $\varphi = 0°$ has the maximum peak compared to the other cases. From the view of the lift mechanism of the thin wing during unsteady motion, lift is definitely related to the incoming velocity as well as the deformation velocity of the wing. Hence, this is now a metric that can be used to quantify the deformation of the inner wing. As shown in Fig. 2, the cases produce significantly different lift coefficients because of the difference in the phase difference of the dynamic trailing-edge flap, and it is this difference in phase difference that leads to the difference in U_{eff} of the effective airfoil shown in Fig. 4. As a result, U_{eff} is considered physically reasonable as a means of measuring the morphing speed of the wing. Furthermore, the lift coefficient can also be corrected by introducing U_{eff} to derive a new lift coefficient (hereinafter referred to as corrected lift coefficient), given by

$$\tilde{C}_L = \frac{L}{\frac{1}{2}\rho(U_{eff} + U_\infty)^2 S^*}. \qquad (7)$$

As shown in Fig. 5, the corrected lift coefficient formula, Eq. (7), indicates that the effective velocity can be used to explain the effect of the dynamic trailing-edge flap on the lift of the flapping-wing model. It is observed that the different curves in Fig. 2 almost coincide when using Eq. (7) in Fig. 5. The corrected lift coefficients at different pitching amplitudes also coincide with each other (see the details in Sec. V of the supplementary material). The numerical results show that the
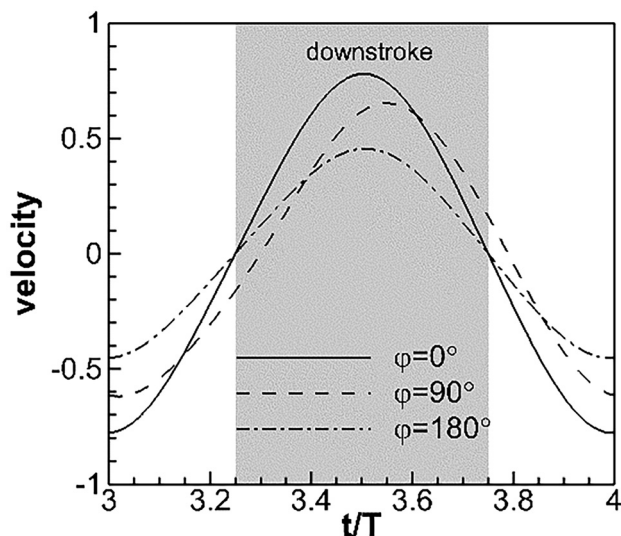

FIG. 4. The z-direction incoming velocity U_{eff} at the quarter-chord point of the effective wing at the spanwise position $y = 0.25$ for three phase-difference cases. The gray and white blocks denote the downstroke and upstroke, respectively.
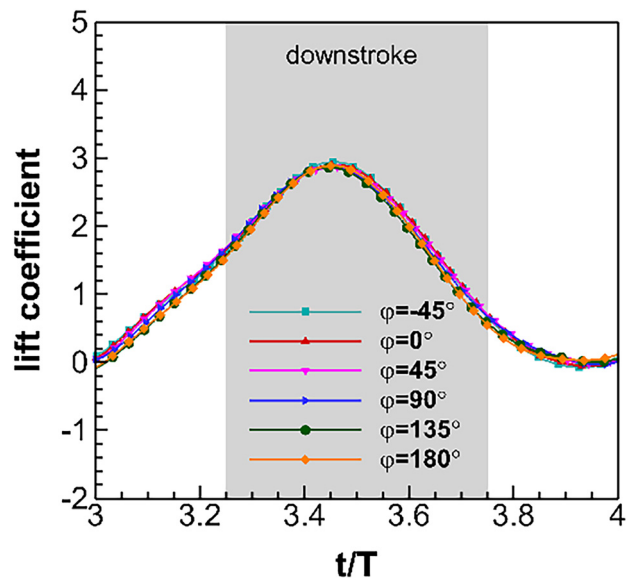

FIG. 5. Corrected lift coefficients at different phase differences. The gray and white blocks denote the downstroke and upstroke, respectively.

corrected lift coefficient formula can be used as a simplified model for predicting trends of lift.

According to Eq. (7), the lift formula can be expressed as $L(t/T, \varphi) = 1/2\rho\tilde{C}_L S^*(U_{eff} + U_\infty)^2$, where U_{eff} can be considered as a function $U_{eff} = U_{eff}(t/T, \varphi)$, with t/T and φ as independent variables. Then, the phase difference achieving the maximum U_{eff} is obtained as $-8.41°$, and according to the previous conclusion, the maximum lift of the wing model can be reached approximately when $\varphi = -8.41°$. The details of the estimation of the phase difference corresponding to the maximum lift can be found in the supplementary material. This numerical result is obtained under the condition ($\varphi = -8.41°$, $AoA = 25°$, $\alpha_0 = \alpha_m = 10°$); the average lift coefficient $C_{L,avg} = 1.60$, and the peak lift coefficient $C_{L,max} = 4.06$. The average lift coefficient and the peak lift coefficient in this case have been improved by 6.29%, and 7.06%, respectively, compared with those in the baseline. In the case with $\varphi = 0°$, there are 6.17% and 6.81% improvements for $C_{L,avg}$ and $C_{L,max}$, respectively, compared with the baseline. Hence, both from the analytical and numerical results, it is found that a suitable negative phase difference is beneficial to improve the lift. Likewise, Cheney et al.[14] observed uropatagium morphing of fruit bats during steady flight, and it can be found that there is a negative phase difference in uropatagium pitching compared to shoulder elevating. In other words, the uropatagium starts the downstroke earlier compared to shoulder elevating during the steady flight of bats.

In summary, this work extracts kinematic characteristics from bat flight to construct a flapping-wing model with a dynamic trailing-edge flap. A series of unsteady lift coefficient with changes in the phase of the dynamic trailing-edge flap are obtained by calculating the flows around the bio-inspired flapping-wing model. After obtaining the relationship between the phase difference of the dynamic trailing-edge flap and the lift, it is found that the phase difference corresponding to obtaining maximum lift is not $0°$, but a negative phase difference

closer to $0°$. A simplified model is proposed to predict the effect of dynamic trailing-edge flap on lift and to explain the relationship between the phase difference of the dynamic trailing-edge flap and lift. Using this model, it can be concluded that the phase difference corresponding to the maximum lift is a negative value close to $0°$, which means that the dynamic trailing-edge flap starts from the downstroke slightly earlier than shoulder elevating to obtain the peak of lift, this phase difference is also consistent with the observation reported in the experiment of bat flight.

SUPPLEMENTARY MATERIAL

See the supplementary material for detailed derivation of the effective velocity U_{eff}, discussion of the phase difference φ corresponding to the maximum lift, and the corrected lift coefficient at different flapping parameters.

ACKNOWLEDGMENTS

AUTHOR DECLARATIONS

Conflict of Interest

The authors have no conflicts to disclose.

Author Contributions

Yixin Chen: Data curation (equal); Formal analysis (equal); Investigation (equal); Methodology (equal); Software (equal); Validation (equal); Visualization (equal); Writing – original draft (equal); Writing – review & editing (equal). **Chunyu Wang:** Methodology (equal); Software (equal); Visualization (equal); Writing – review & editing (equal). **Jing-Shan Zhao:** Conceptualization (equal); Investigation (equal); Supervision (equal); Writing – review & editing (equal). **Shizhao Wang:** Conceptualization (equal); Funding acquisition (equal); Methodology (equal); Resources (equal); Software (equal); Supervision (equal); Writing – original draft (equal); Writing – review & editing (equal).

DATA AVAILABILITY

The data that support the findings of this study are available from the corresponding authors upon reasonable request.

REFERENCES

[1]P. Henningsson, L. Jakobsen, and A. Hedenström, "Aerodynamics of manoeuvring flight in brown long-eared bats (*Plecotus auritus*)," J. R Soc. Interface **15**, 20180441 (2018).

[2]A. Hendenström and L. C. Johansson, "Bat flight," Curr. Biol. **25**, 399–402 (2015).

[3]U. M. Norberg, "Allometry of bat wings and legs and comparison with birds' wings," Philos. Trans. R. Soc. **292**, 359–398 (1981).

[4]A. L. Thomas and G. K. Taylor, "Animal flight dynamics I. Stability in gliding flight," J. Theor. Biol. **212**, 399–424 (2001).

[5]F. Beaumont, S. Murer, F. Bogard, and G. Polidori, "Aerodynamics of a flapping wing as a function of altitude: New insights into the flight strategy of migratory birds," Phys. Fluids **33**, 127118 (2021).

[6]Y. Xue, X. Cai, and H. Liu, "Effects of wing–body interaction on hawk moth aerodynamics and energetics at various flight velocities," Phys. Fluids **34**, 051915 (2022).

[7]W. Maybury, J. Rayner, and L. B. Couldrick, "Lift generation by the avian tail," Proc. R Soc. Lond. B. **268**, 1443–1448 (2001).

[8]R. Bullen and N. L. McKenzie, "Bat airframe design: Flight performance, stability and control in relation to foraging ecology," Aust. J. Zool. **49**, 235–261 (2001).

[9]A. Hendenström, L. C. Johansson, and G. R. Spedding, "Bird or bat: Comparing airframe design and flight performance," Bioinspir. Biomim. **4**, 015001 (2009).

[10]J. D. Gardiner, G. Dimitriadis, J. R. Codd, and R. L. Nudds, "A potential role for bat tail membranes in flight control," PloS ONE **6**, e18214 (2011).

[11]R. A. Adams, E. R. Snode, and J. B. Shaw, "Flapping tail membrane in bats produces potentially important thrust during horizontal takeoffs and very slow flight," PloS ONE **7**, e32074 (2012).

[12]A. Ramezani, S. Chung, and S. Hutchinson, "A biomimetic robotic platform to study flight specializations of bats," Sci. Rob. **2**, eaal2505 (2017).

[13]J. A. Cheney, J. C. Rehm, S. M. Swartz, and K. S. Breuer, "Bats actively modulate membrane compliance to control camber and reduce drag," J. Exp. Biol. **225**(14), jeb243974 (2022).

[14]J. A. Cheney, D. Ton, N. Konow, D. K. Riskin, K. S. Breuer, and S. M. Swartz, "Hindlimb motion during steady flight of the lesser dog-faced fruit bat, *Cynopterus brachyotis*," PloS ONE **9**, e98093 (2014).

[15]C. Wang, Y. Liu, D. Xu, and S. Wang, "Aerodynamic performance of a bio-inspired flapping wing with local sweep morphing," Phys. Fluids **34**, 051903 (2022).

[16]T. Liu, K. Kuykendoll, R. Rhew, and S. Jones, "Avian wing geometry and kinematics," AIAA J. **44**, 954–963 (2006).

[17]E. Ajanic, M. Feroskhan, S. Mintchev, F. Noca, and D. Floreano, "Bioinspired wing and tail morphing extends drone flight capabilities," Sci. Robot. **5**, eabc2897 (2020).

[18]X. Lang, B. Song, W. Yang, and X. Yang, "Effect of spanwise folding on the aerodynamic performance of three-dimensional flapping flat wing," Phys. Fluids **34**, 021906 (2022).

[19]S. Wang, X. Zhang, G. He, and T. Liu, "Lift enhancement by dynamically changing wingspan in forward flapping flight," Phys. Fluids **26**, 061903 (2014).

[20]C. Wang, Z. Xu, X. Zhang, and S. Wang, "Optimal reduced frequency for the power efficiency of a flat plate gliding with spanwise oscillations," Phys. Fluids **33**, 111908 (2021).

[21]S. Wang, G. He, and X. Zhang, "Lift enhancement on spanwise oscillating flat-plates in low-Reynolds-number flows," Phys. Fluids **27**, 061901 (2015).

[22]S. Wang and X. Zhang, "An immersed boundary method based on discrete stream function formulation for two- and three-dimensional incompressible flows," J. Comput. Phys. **230**, 3479–3499 (2011).

[23]S. Wang, G. He, and X. Zhang, "Parallel computing strategy for a flow solver based on immersed boundary method and discrete stream-function formulation," Comput. Fluids **88**, 210–224 (2013).

[24]C. Li, H. Dong, and G. Liu, "Effects of a dynamic trailing-edge flap on the aerodynamic performance and flow structures in hovering flight," J. Fluids Struct. **58**, 49–65 (2015).

[25]H. Dai, H. Luo, and J. F. Doyle, "Dynamic pitching of an elastic rectangular wing in hovering motion," J. Fluid Mech. **693**, 473–499 (2012).